Performance improved full-duplex millimeter-wave signal generation with tunable FMF by incorporating a bit walk-off effect compensation

R. ARYA, JOSEPH ZACHARIAS*
Fiber Optics Lab, Department of Electronics and Communication Engineering, Rajiv Gandhi Institute of Technology, Kerala-686501, India

This paper proposes a full duplex system for the generation of millimeter-wave signals at different frequencies by tuning the frequency multiplication factor. The system is capable of transmitting different information at required data rate through the mm-wave signals according to their application. A uniform fiber Bragg grating based acousto-optic tunable filter (UFBG-based-AOTF) is employed for the generation of tunable millimeter-wave signals and this reduces the system complexity by alleviating the structured Mach-Zehnder modulators (MZM). The uplink transmission is realized by reusing the downlink optical carrier which makes the proposed system cost-effective and reliable. Besides, the bit walk-off effect which is occurred when a modulated double sideband signal gets transmitted through the fiber is addressed and compensated and it helps in improving the transmission performance to more fiber distance. A simulation link is built for the generation of tunable millimeter-wave signals with data rates of 1 Gbps, 4 Gbps and 5 Gbps over 20 GHz, 40 GHz and 60 GHz respectively. Simulation results show that the transmission distance is increased to 50 km and the bit error rate performance is improved in the proposed system when compared to the previous systems where the transmission distance is limited to about 15 km.

(Received August 9, 2018; accepted December 10, 2019)

Keywords: Acousto-optic tunable filter (AOTF), Bit walk-off effect, Different data rates, Full duplex communication, Optical millimeter-wave, Uniform fiber Bragg grating (UFBG).

1. Introduction

The current decade is facing a pretty remarkable challenge which is the perpetual growth in the increasing demand for a spectrum to meet the increasing global communication requirements. The spectrum deficiency induces to have less bandwidth for every user which causes slower service as well as more downed connections. In order to avoid the wireless traffic congestion, millimeter-wave (mm-wave) transmission is the most promising method which presents large bandwidth at very high frequencies. This large bandwidth is directly proportional to high data transfer rates and thus make possible the bandwidth-intensive applications like 10 Gbps file transfer, high-definition (HD) wireless video streaming, real-time gaming and so on. The short wavelength range of mm-wave signals allows smaller antenna size. Thus multi-antenna systems can be built which enables directional transmission and helps in overcoming the signal transmission losses. Besides, there will not be any disturbance to the prevailing radio systems because of the huge bandwidth. As a result, mm-wave systems offer high immunity to jamming and interference which enables them to use in short range secure wireless local area network (WLAN) communications. Most relevantly, the mm-wave systems offer high reliability with low latency and constant connectivity- anytime and anywhere [1].

Compared to electronic-based techniques of mm-wave signal generation, optical methods offer simpler configuration and extremely wide bandwidths. It reduces the signal attenuation due to atmospheric water molecules and oxygen. So radio over fiber (RoF) is a promising method for the generation and distribution of mm-wave signals[2]. For the generation of optical mm-wave signals, several methods are developed recently [3]. Among them, a simple method is to directly modulate a high-speed laser diode by an mm-wave carrier source. But in this method, as the intensity of light gets modulated, the wavelength also gets modulated which results in a limitation of transmission distance by this chirp induced dispersion. Since the modulation bandwidth of the laser limits the modulating signal frequency, the maximum bandwidth modulated can reach only a few tens of GHz at the very best.

In the optical heterodyne technique [4], two optical carriers which are separated by the desired frequency are produced from either two stabilized lasers or one laser with an external modulator and are beaten in a square-law photodetector for the generation of mm-wave signals. For the two optical carriers, the offset frequency must be stable and their phases are to be correlated. So to generate a high quality mm-wave signal, the phase difference as well as frequency offset between the two optical carriers has to be precisely controlled.

Various methods like optical phase/frequency locked loop (OPLL/OFLL) and optical injection locking[5] are thus proposed to improve the signal quality. Both these methods involve a feedback system to compare the generated mm-wave signal with a reference signal which is able to track phase/frequency variations. But these systems require lasers with narrow linewidth and complex structures for giving better results.

The external modulation method of mm-wave generation [6] has a great capacity for the accurate generation of signals in the mm-wave band. This method uses a continuous wave (CW) laser along with an external modulator like MZM so that an optical carrier and harmonics of each order are generated. In this method, a mm-wave signal is generated by the beating of the optical harmonics at a PD which are selected by either filtering or biasing the MZM properly. Hence the generated mm-wave signal depends on a frequency multiplication factor (FMF) which in turn depends on the frequency of the drive signal and the biasing of MZM. So the generated signal suffers from the distortion due to the non-linearity of MZM as well as a bias drifting problem which causes due to the improper biasing of MZM. This reduces the robustness of the system.

In [7], a mm-wave generation technique is demonstrated by employing n cascaded external intensity modulators so that the frequency of the generated mm-wave signal is 2n times that of the RF drive signal. However this method needs proper regulation of phase relation between RF signals on every n external modulator. To further improve the signal quality and to generate higher frequency mm-wave signals, structured or integrated MZMs are employed for the realization of quadrupling [8] as well as octupling [9] mm-wave signal generation. These method [8,9] generates high spectral purity mm-wave signals and a high optical sideband suppression ratio (OSSR) but with high complexity and poor stability. Moreover when the generated mm-wave signal transmits through a single mode fiber (SMF), the fiber dispersion effects reduce the data rate that can be achieved best without attenuation [10,11].

To realize the tunable FMF, a technique of multiple-wavelength selection can be employed which uses an integration of a phase modulator (PM) and an external modulator like either an MZM [12] or an electro-absorption modulator (EAM) [13] to generate many multiple wavelength signals. Two optical sidebands with the desired wavelength spacing is selected by a wavelength selective filter which will get mixed at a PD. But the frequency tuning can be achieved only by adjusting more than two parameters simultaneously which increases system complexity and dc bias-shifting problem occurs here leads to poor system robustness.

In [14], mm-wave signals are generated by quadrupling the frequency of input local oscillator without using filters. Here unwanted Optical Sideband Suppression Ratio (OSSR) and Radio Frequency Spurious Sideband Suppression Ratio (RFSSR) are improved. But bitwalk-off effect is not considered. Moreover in order to achieve tunability in mm-wave signal generation, the local oscillator frequencies have to be tuned and biasing parameters of the MZM have to be varied carefully as in [15] and [16]. Ref. [17] introduces a generalized method for the generation of tunable microwave signals based on two cascaded Mach-Zehnder modulators. FMF of four, six and eight can be implemented with this technique. But this method also involves proper controlling of the power and bias parameters of the MZM in order to select the desired sidebands which cause bias drifting problems.

Another frequency-tunable method for the generation of subterahertz waves based on electrooptical modulation is demonstrated in [18]. Since it uses a polarization modulator which needs no biasing, the bias drift problem can be effectively eliminated. For mm-wave signal generation, an optical notch filter is used which removes the first order sidebands. Frequency tenability is achieved by tuning the frequency of the microwave drive signal without tuning the notch filter. Thus the maximum frequency of the signals that can be generated by this method is limited by the bandwidth of the polarization modulator and photodetector. Ref. [19] introduces a similar frequency tunable method for microwave generation which uses an optical comb generator and MF tunable by adjusting the central frequency of a single-passband microwave photonic filter (MPF). In this system, in order to achieve frequency-tunability, frequency of the microwave reference signal is changed along with the tuning of the passband of the MPF accordingly.

Most of the above mentioned methods achieve frequency tunability by tuning the frequency of the drive signal which limits the highest frequency that can be generated since the bandwidth of the modulators and photodetectors is limited. But in [20], a tunable mm-wave signal generation method by employing an UFBG-based-AOTF is demonstrated. The UFBG-based-AOTF is a filter used for the selection of target sidebands with desired wavelength spacing from a multiple-wavelength signal generated by a dual drive-MZM (DD-MZM) and gets beaten at PD to realize a tunable FMF of 2n (n = 1, 2 and 3). In this method, the complexity of the system and the frequency prerequisite of modulator and oscillator is greatly reduced. By the use of FBG, the dispersion effects can also be mitigated. But in this system, each generated mm-wave frequency band carries the same information at 256 Mb/s data rate and when this double sideband (DSB) signal gets transmitted across a fiber, bit walk-off effect occurs which is not discussed in [20].

This paper proposes a full duplex tunable mm-wave signal generation in which the full duplex communication is realized by wavelength reuse [21], hence it reduce the need of a high-frequency laser source at the base station (BS) and makes the system cost-effective. The proposed system employs a UFBG-based-AOTF for the generation of mm-wave signal and for realizing the tunable FMF, the frequency of the acoustic wave supplied to the UFBG-based-AOTF is tuned or adjusted. Compared to [20], the proposed system offers the possibility of transmitting different information at a data rate through each generated mm-wave signal as required by its application. The bit walk-off effect which occurs when the modulated DSB

signal is transmitted across the fiber is addressed as well as compensated in the proposed system which improves the transmission performance. From the simulation results, it can be shown that the transmission distance is increased to 50 km after bit walk-off effect compensation which was about 10 to 20 km only before the compensation of the effect. BER performance was also increased to several times in the proposed system when compared to previous systems of mm-wave generation.

The organization of the paper is described as follows: In section II, after explaining the principle of UFBG-based-AOTF, the mechanism of the proposed full duplex tunable mm-wave signal generation system is detailed. This is followed by a section which explains the simulation setup needed to validate our proposal. Finally in section IV, the obtained results are analyzed and compared with other systems to prove its advantages and section V briefly concludes the work.

2. Principle and concept of the proposed scheme

In this section, the working principle of the UFBG-AOTF is described in the first part which is followed by an explanation of the mechanism of the full duplex mm-wave signal generation with tunable FMF. In the mechanism, after analyzing the transmission of the system, a bit walk-off effect compensation is proposed to make the system free from the involved transmission impairments.

2.1. UFBG-based-AOTF

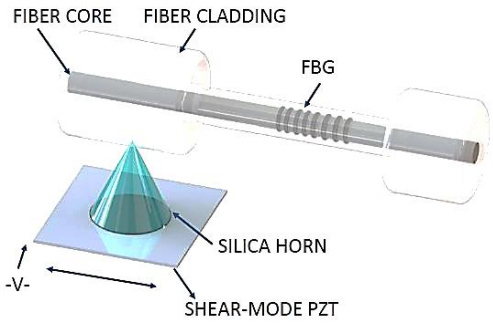

Fig. 1. UFBG based AOTF

Fig. 1 shows an all fiber uniform fiber Bragg grating based acousto-optic tunable filter (UFBG based AOTF) which has been used in wavelength selectivity in the proposed full duplex tunable mm-wave signal generation system. As shown in the Fig. 1, the UFBG based AOTF is composed of a shear mode piezoelectric ceramic transducer (PZT), an acoustic silica horn and a uniform fiber Bragg grating (UFBG) inscribed on an SMF.

When an RF signal is applied to the PZT in a direction perpendicular to the direction of polarization, the PZT gets actuated in the shear mode which results in the formation of a longitudinal acoustic wave (AW) and the acoustic wavelength is determined by the frequency of the applied RF signal. It is amplified by the acoustic silica horn and coupled to the fiber. The longitudinal AW produces a strain which causes the UFBG to have regions of periodic expansion and compression with commensurable differences in refractive index. This leads to the production of additional reflections on either sides of the grating reflection peak in the reflection spectrum of modulated UFBG while comparing to the single reflection peak spectrum of unmodulated UFBG. This is explained in Fig. 2.

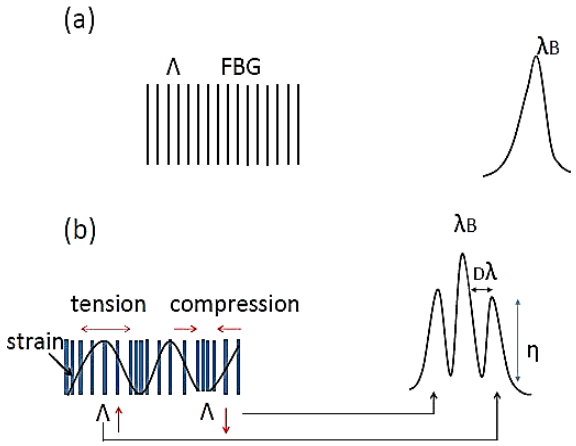

Fig. 2. Reflection spectrum of UFBG (a) Unmodulated UFBG (b) Modulated UFBG with acoustic wave

The wavelength spacing between primary and secondary reflection peaks in the spectrum can be adjusted by tuning the acoustic frequency. The working principle of the UFBG-based-AOTF states that "wavelength of the diffracted light depends on acoustic frequency." Since the acoustic wavelength depends on the frequency of the RF signal, any alteration in the RF signal frequency results in a change in the wavelength of diffracted light. Thus by tuning the applied frequency and making the secondary reflections of the UFBG-based-AOTF to get aligned with the target sidebands of the MZM output, they can be filtered out.

2.2. Mechanism of the scheme

The proposed full duplex system for mm-wave signal generation with a tunable FMF is shown using the block diagram in Fig. 3. At the central station (CS), a tunable laser (TL) with narrow linewidth, about 1 MHz, is used to generate a continuous lightwave at 1544.4 nm. Since the CW has no bandwidth and all its energy is concentrated towards a single frequency, it does not get involved with transmissions on other frequencies. A radio-frequency (RF) signal at 10 GHz is used to modulate the carrier at 194.116 THz by a Dual-drive Mach-Zehnder modulator (DD-MZM) and the output is shown in Fig. 3 a. In order to achieve optical DSB modulation, the DD-MZM is biased at quadrature bias point (harmonic content is low) and the difference in phase between both RF branches is set to be π [20].

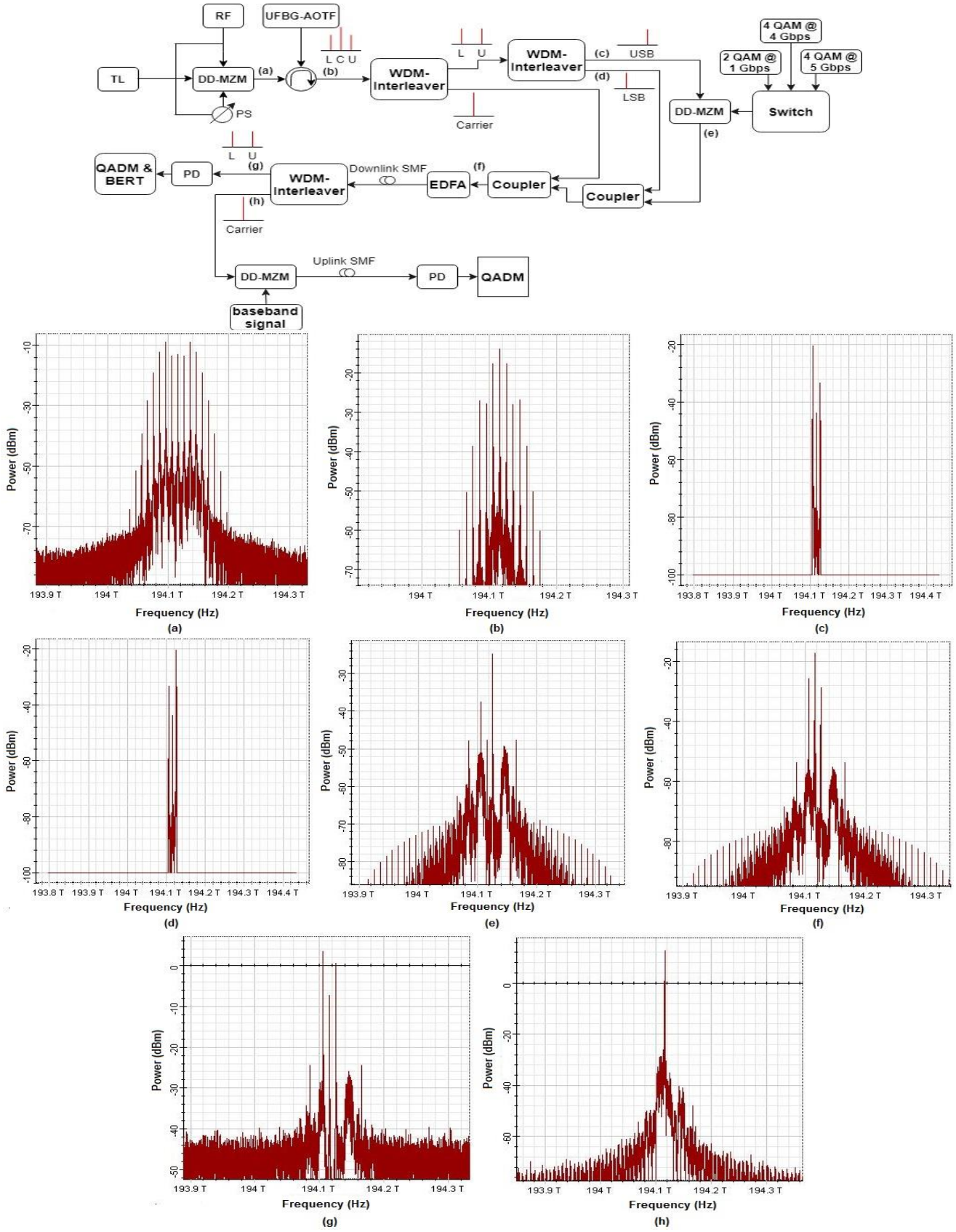

Fig. 3. Full duplex tunable mm-wave signal generation to transmit three different data through each signal with bit walk-off effect compensation and outputs obtained at points a, b, c, d, e, f, g and h. (TL: tunable laser, DD-MZM: dual-drive Mach-Zehnder modulator, PD: photodetector, QADM: quadrature amplitude demodulator, BERT: bit-error-rate tester)

Let us consider that the input light from the laser with a central wavelength of $\lambda_c = {2\pi c}/{\omega_c} = {c}/{f_c}$ can be expressed as $E_c(t) = E_0 e^{j\omega_c t}$ and an electrical RF carrier at $V_m(t) = V_{RF}\cos\omega_m t$ modulates the lightwave. Since the LN-MZM has a characteristic of non-linear response, the output lightwave consists of multiple sidebands along with the carrier, which is shown in Fig. 3 b.

And it is expressed as,

$$\begin{aligned} E_{M,out} &= E_0 e^{j\omega_c t}\left[e^{+j\pi\frac{V_m}{2V_\pi}} + e^{-j\pi\frac{V_m}{2V_\pi}}\right] \\ &= E_0 e^{j\omega_c t}\left[\sum_{k=-\infty}^{\infty}(-1)^k J_k(m) e^{jk\omega_m t}\right] \\ &= E_0\left[\sum_{k=-\infty}^{\infty}(-1)^k J_k(m) e^{j(\omega_c + k\omega_m)t}\right] \\ &= E_0\big[J_0(m)e^{j\omega_c t} - J_1(m)\,(e^{j(\omega_c-\omega_m)t} \\ &\quad + e^{j(\omega_c+\omega_m)t}) + J_2(m)\,(e^{j(\omega_c-2\omega_m)t} \\ &\quad + e^{j(\omega_c+2\omega_m)t}) - J_3(m)\,(e^{j(\omega_c-3\omega_m)t} \\ &\quad + e^{j(\omega_c+3\omega_m)t}) + ..\big] \end{aligned} \tag{1}$$

where the RF modulation index is,

$$m = \pi\frac{V_{RF}}{V_\pi} \tag{2}$$

V_{RF} denote RF modulation signal voltage magnitude and V_π is half switch MZM voltage [22]. $J_n(.)$ is first kind Bessel function of nth order. Since Equation 1 shows that the DD-MZM output constitutes an optical carrier with each order sidebands symmetrically located around the carrier, the amplitude of carrier and all sidebands can be varied by varying V_{RF} or equivalently m.

ω_m corresponds to the frequency spacing across carrier and primary sidebands in DD-MZM output. So in order to realize a tunable FMF of 2n, the UFBG-based-AOTF selects the target sidebands with a frequency spacing of $2\omega_m$, $4\omega_m$ and $6\omega_m$ for n=1,2 and 3 respectively. Thus high frequency mm-wave signals whose frequency is 2n times the frequency of input RF drive signal can be generated which significantly reduces the frequency requirement of modulators and oscillators used in the proposed system.

2.2.1. Analysis of downlink transmission performance

Consider that a 4 Gbps 4 QAM data at 40 GHz is modulated on to the downlink signal at both second-order sidebands which results in an output,

$$\begin{aligned} E_{d,out}(t) &= E_0 J_0(m) e^{j\omega_c t} \\ &\quad + \eta D(t) E_0 J_2(m)[e^{j(\omega_c-2\omega_m)t} \\ &\quad + e^{j(\omega_c+2\omega_m)t}] \end{aligned} \tag{3}$$

where the first part $E_0 J_0(m) e^{j\omega_c t}$ denotes the unmodulated carrier and the second part denotes modulated second order sidebands with D(t) denotes the data modulated on the signal and η is the attenuation caused by data modulation.

As the modulated DSB signal passes through an SMF with chromatic dispersion effects, a different phase shift in both phase and time has to be suffered by each sideband data and this forces the data bits to walk off from one another with respect to the length of FMF [23,24]. Also, when a DSB signal transmits through a fiber, both sidebands possess different velocities. This leads to the lightwave at the fiber output as,

$$\begin{aligned} E_{d,out}(t,z) &= E_0 e^{-\frac{\kappa z}{2}} J_0(m) e^{j\omega_c(t-t_0)} \\ &\quad + \eta E_0 e^{-\frac{\kappa z}{2}} J_2(m) \\ &\quad [D(t-t_{-2}) e^{j(\omega_c-2\omega_m)(t-t_{-2})} \\ &\quad + D(t-t_{+2}) e^{j(\omega_c+2\omega_m)(t-t_{+2})}] \end{aligned} \tag{4}$$

where the ± 2sidebands carries the code pulses $D(t-t_{-2})$ and $D(t-t_{+2})$ and the constant of transmission of lightwave at an angular frequency ω is denoted as $\beta(\omega)$ with,

Shift in carrier, $t_0 = \frac{\beta(\omega_c)}{\omega_c} z$

Shift in sidebands, $t_{\pm 2} = \frac{\beta(\omega_c \pm 2\omega_m)}{\omega_c \pm 2\omega_m} z$

Thus Equation 4 implies,

$$\begin{aligned} E_{d,out}(t,z) &= E_0 e^{-\frac{\kappa z}{2}} J_0(m) e^{j(\omega_c t - \beta(\omega_c) z)} \\ &\quad + \eta E_0 e^{-\frac{\kappa z}{2}} J_2(m) \\ &\quad [D(t-(\omega_c-2\omega_m)^{-1}\beta(\omega_c-2\omega_m)z) \\ &\quad e^{j((\omega_c-2\omega_m)t-\beta(\omega_c-2\omega_m)z)} \\ &\quad + D(t-(\omega_c+2\omega_m)^{-1}\beta(\omega_c+2\omega_m)z) \\ &\quad e^{j((\omega_c+2\omega_m)t-\beta(\omega_c+2\omega_m)z)}] \end{aligned} \tag{5}$$

where κ is the optical power attenuation along the fiber. So it can be made clear from Equation 5 that the data bits carried by ± 2 sidebands, $D(t-t_{+2})$ and $D(t-t_{-2})$, walk-off from one another as they get traveled across a fiber.

At the base station (BS) end, the uplink optical carrier and downlink mm-wave signal is separated from the received signal using a wavelength division multiplexer (WDM) interleaver. The PD detects the separated downlink signal and mm-wave signals with a tunable FMF of 2n (n=1, 2, 3) can be generated. The separated mm-wave signal can be expressed as,

$$\begin{aligned} E_{MM-W}(t,z) &= \eta E_0 e^{-\frac{\kappa z}{2}} J_2(m) \\ &\quad [D(t-t_{-2}) e^{j(\omega_c-2\omega_m)(t-t_{-2})} \\ &\quad + D(t-t_{+2}) e^{j(\omega_c+2\omega_m)(t-t_{+2})}] \end{aligned} \tag{6}$$

which is detected by a PD to generate a mm-wave signal at frequency $4\omega_m$ and the photocurrent is always proportionate to the square of the optical electric field. The PD output can be expressed as,

$$I_{out}(t,z) = \mu |E_{MM-W}(t,z)|^2$$

with μ being the proportionality constant which is called responsivity of the PD.

$$\begin{aligned} I_{out}(t,z) = \mu\eta^2[&D(t-t_{+2})^2 + D(t-t_{-2})^2 \\ &+2D(t-t_{+2})D(t-t_{-2}) \\ &cos2\omega_m(t-\beta(\omega_c)z)] \end{aligned} \tag{7}$$

where,

$$t_{\pm 2} = \frac{\beta(\omega_c \pm 2\omega_m)}{\omega_c \pm 2\omega_m} z$$

It contains both RF signal and baseband signal in such a way that the baseband signal amplitude is proportionate to the sum of squares of code pulses over ± 2 sidebands while the RF signal corresponds to the product of code pulses over$\pm$2sidebands. As the signal transmission distance is increasing, the baseband pulse expands while RF pulse narrows which ascertain the existence of the bit walk-off effect.

2.2.2. Bit walk-off effect compensation

In the proposed system, in order to deal with bit walk-off effect only one among the two n^{th} order sidebands (± 2) are modulated by the QAM modulating signal instead of modulating both sidebands. For the implementation as shown in Figure 3, a WDM interleaver is used to separate either LSB or USB from the signal and then the data is modulated onto either of them. Consider second-order sidebands and let the data be modulated onto the USB at $(f_c + f_m)$. Then the modulated signal after coupling with carrier and unmodulated LSB becomes,

$$\begin{aligned} E_{d,out}(t) = &E_0 J_0(m) e^{j\omega_c t} \\ &+ E_0 J_2(m) e^{j(\omega_c - 2\omega_m)t} \\ &+ \eta E_0 J_2(m) D(t) e^{j(\omega_c + 2\omega_m)t}] \end{aligned} \tag{8}$$

The light wave at fiber output becomes,

$$\begin{aligned} &E_{d,out}(t,z) \\ &= E_0 e^{-\frac{\kappa z}{2}} J_0(m) e^{j(\omega_c t - \beta(\omega_c)z)} \\ &+ E_0 e^{-\frac{\kappa z}{2}} J_2(m) [\, e^{j((\omega_c - 2\omega_m)t - \beta(\omega_c - 2\omega_m)z)} \\ &\quad +\eta D(t-(\omega_c + 2\omega_m)^{-1}\beta(\omega_c + 2\omega_m)z) \\ &\quad e^{j((\omega_c + 2\omega_m)t - \beta(\omega_c + 2\omega_m)z)}] \end{aligned} \tag{9}$$

where δ is the phase difference introduced in between both the sidebands due to the difference in light paths and it leads to the broadening of beating RF spectrum. Hence at the BS end, the separated downlink mm-wave signal becomes,

$$\begin{aligned} E_{MM-W}(t,z) = &E_0 e^{-\frac{\kappa z}{2}} J_2(m) \\ &[\, e^{j((\omega_c - 2\omega_m)t - \beta(\omega_c - 2\omega_m)z)} \\ &+\eta D(t-(\omega_c + 2\omega_m)^{-1}\beta(\omega_c + 2\omega_m)z) \\ &e^{j((\omega_c + 2\omega_m)t - \beta(\omega_c + 2\omega_m)z)}] \end{aligned} \tag{10}$$

Equivalently the photocurrent becomes,

$$\begin{aligned} I_{out}(t,z) &= \mu |E_{MM-W}(t,z)|^2 \\ &= \mu\eta^2[D(t-t_{+2})^2 + 1 \\ &\quad +2D(t-t_{+2}) cos2\omega_m(t-\beta(\omega_c)z) + \delta] \end{aligned} \tag{11}$$

In Equation 11,$D(t-t_{-2}) = 0$and thus it makes clear that when data modulates onto only one sideband, the system does not have any walk off of the code bits as they travel across the fiber. Thus, expansion of baseband signal and narrowing of RF signal gets significantly reduced as compared to Equation 7.

Finally, the baseband signal is abstracted from the RF carrier to check transmission performance and the BER performance is evaluated.

2.2.3 Uplink transmission

At the BS end, as explained earlier, the uplink optical carrier is separated from the downlink mm-wave signal by a WDM interleaver. The separated optical carrier can be expressed as,

$$E_c(t,z) = E_0 e^{-\frac{\kappa z}{2}} J_0(m) e^{j(\omega_c t - \beta(\omega_c)z)} \tag{12}$$

which can be utilized for the transmission of upstream signals to the CS. Thus the need of a high frequency LO at the base station can be avoided which makes the proposed system more reliable and cost-effective.

In order to send an upstream signal, an mm-wave signal at frequency $\omega_u$is sent by the user terminal to the BS wirelessly. The mm-wave signal is then downconverted to a baseband signal $S_u(t)$ which is the upstream data that modulates the optical carrier at ω_c.The modulated carrier is represented as,

$$E_{c,d}(t,z) = E_0 e^{-\frac{\kappa z}{2}} J_0(m) \eta U(t) e^{j(\omega_c t - \beta(\omega_c)z)} \tag{13}$$

where U(t) is the upstream data send over the carrier back to the CS along a fiber. At the CS, a PD is used to detect the received optical mm-wave signal and converted back to an electrical signal.

3. Simulation setup

In order to verify the design of the proposed scheme, a simulation model for the generation of a full duplex mm-wave signal with tunable FMF of 2n (for n= 1,2,3) is built by an Optisystem 14 software as shown in Fig. 3. The Optisystem is designed to be an ergonomic platform which

provides an interface to implement the design and the simulation results are effective as proof or evidence. A continuous light wave at a center frequency of 194.116 THz is emitted from a tunable laser with a 1 MHz linewidth and is injected to a DD-MZM. The DD-MZM is biased at its quadrature bias point and driven by a 10 MHz RF signal with a 180^0phase shift between the two arms. Equation 1 shows that MZM output spectrum composed of an optical carrier with multiple-wavelength sidebands symmetrically located around it which is shown in Fig. 3 a. The MZM output is then filtered by a UFBG-based-AOTF which is connected to the port 2 of an optical circulator. The central frequency of the UFBG-based-AOTF has to be set at 194.116 THz and the bandwidth is varied as 20 GHz, 40 GHz and 60 GHz for n=1,2 and 3 respectively with an insertion loss of around 1 dB. The port 3 of the circulator gives the filtered output signal which is shown in Fig. 3 b. Using a WDM interleaver, the USB and LSB signals are separated from the DSB-FC signal which are shown in Fig. 3 c and Fig. 3 d respectively. For the WDM interleaver, the center frequency of the first filter and the frequency spacing between the first filter and the other filter has to be set in order to separate the wavelength components. The USB signal is then modulated by either of the three data information at 1 Gbps, 4 Gbps or 5 Gbps as required by the application which is shown in Fig. 3 e. The modulated USB signal is then coupled to the unmodulated LSB which are further coupled to the carrier using an optical coupler and the resultant signal is shown in Fig. 3 f and an erbium doped fiber amplifier (EDFA) with a gain of 5 dB is used for the amplification of the signal before transmitting it through an SMF of 50 km length. At the receiver side, the downlink signal is separated from the uplink carrier by a WDM interleaver which is shown in Fig. 3 g and Fig. 3 h. A PIN photodetector detects the downlink signal to generate mm-wave signals at 20 GHz, 40 GHz, and 60 GHz. Higher frequency mm-wave signals can also be generated by implementing higher FMF of 8, 10 and so on. The uplink carrier is then modulated with an uplink data using a DD-MZM and further transmitted to the CS via a SMF.

At the CS, the PD detects the uplink mm-wave signal and thus converts the optical signal to an electrical signal. The simulation was conducted using 8192 samples in total with a 128 sequence length and 64 samples per bit. SMF has a dispersion coefficient of 16.75 ps/nm/km and an attenuation coefficient of 0.2 dB/km.

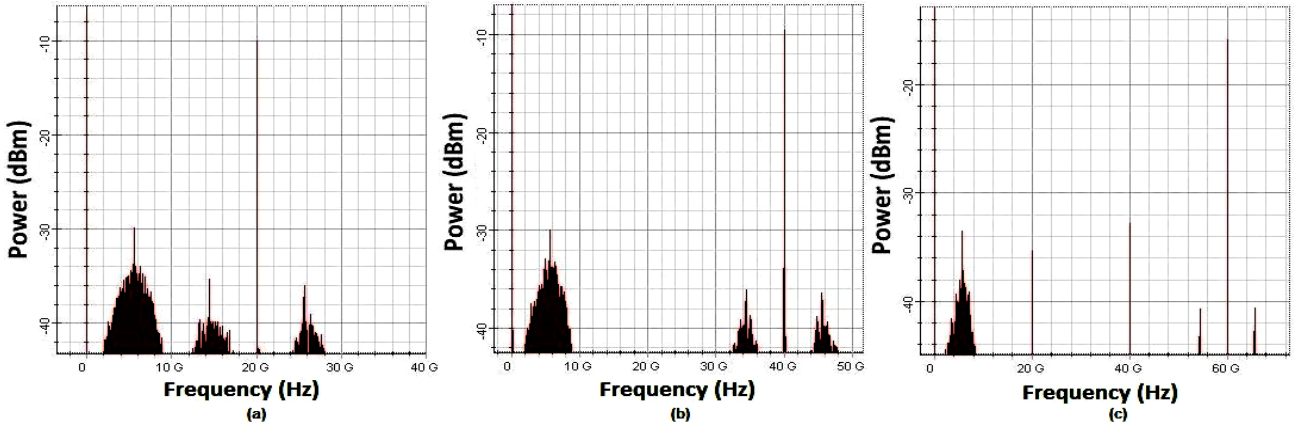

Fig.4. Electrical spectrum showing mm-wave signals generated with FMF (a) 2 (b) 4 and (c) 6.

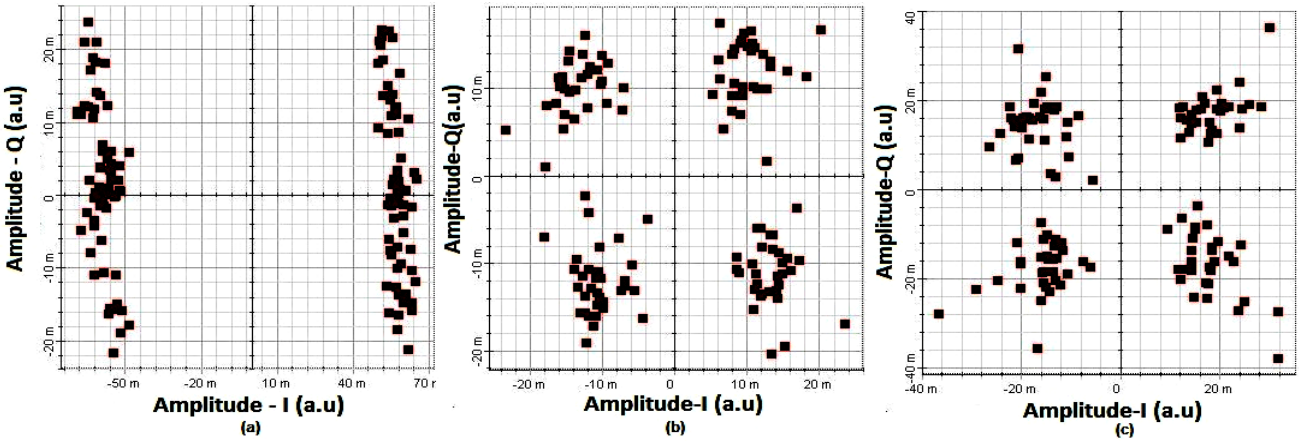

Fig. 5. Constellation obtained (i) after demodulating 20 GHz with a 2 QAM data at 1 Gbps, (ii) after demodulating 40 GHz with a 4 QAM data at 4 Gbps and (iii) after demodulating 60 GHz with a 4 QAM data at 5 Gbps

4. Results and discussion

Fig. 4 a, b and c shows the electrical spectrum of the downlink mm-wave signals generated at 20 GHz, 40 GHz and 60 GHz respectively.

Fig. 4 clearly depicted that the extinction ratio is about 20 dB for 20 GHz and 40 GHz mm-wave signals which will get reduced as frequency of the mm-wave signal gets increased. In order to examine the downlink transmission performance of the system, the downlink photodetector output signal is coherently demodulated to the baseband signal using a local oscillator having the frequency of the generated mm-wave. Fig. 5 shows the constellation diagrams obtained after demodulating the mm-wave signal generated. Compared to the ideal case, distortions and noises can be noticed in the received constellation in Fig. 5.

4.1. Comparison between the proposed system having bit walk-off effect compensation and the system without having bit walk-off effect compensation

The eye diagram comparison curves for the downlink transmission of the system over different lengths of SMF for a full duplex system without bit walk-off effect compensation and with bit walk-off effect compensation are shown in Fig. 6 and Fig. 7 respectively and the BER curves of the above-said systems are compared in Fig. 8.

An error-free performance of the system is assured by the clear opening of the eye diagrams. For a DSB modulated system without bit walk-off effect compensation, the code shift is evaluated among the upper and lower sidebands for different fiber lengths. After analyzing the eye diagrams in Figure 6 which are obtained before compensating the bit walk-off effect from the system, it's observed that at 0 km fiber distance, since the coded data bits on each sideband gets completely overlapped with each other, a clear and open eye diagram is obtained as in Fig. 6 a. It shows the absence of bit walk-off effect. But as the distance increases, dispersion effects in the fiber causes the data bits on each sideband to walk-off from each other which degrades the system performance. This is shown as the distortion in eyediagrams as it moves from Fig. 6 b to d. But after compensating the bit walk-off effect in the proposed system, eyediagrams are obtained as shown in Figure 7. These eyediagrams show an error-free performance constantly over a fiber distance upto 60 km. This is because the code shifting gets highly reduced as the data modulates onto only upper sideband. Thus on the eye diagram a constant width is maintained by every bit and there is no significant eye closure over a transmission distance up to 60 km as in Fig. 7 a to d, i, e.; bit walk-off effect is effectively reduced and better transmission performance is maintained up to a distance of 60 km.

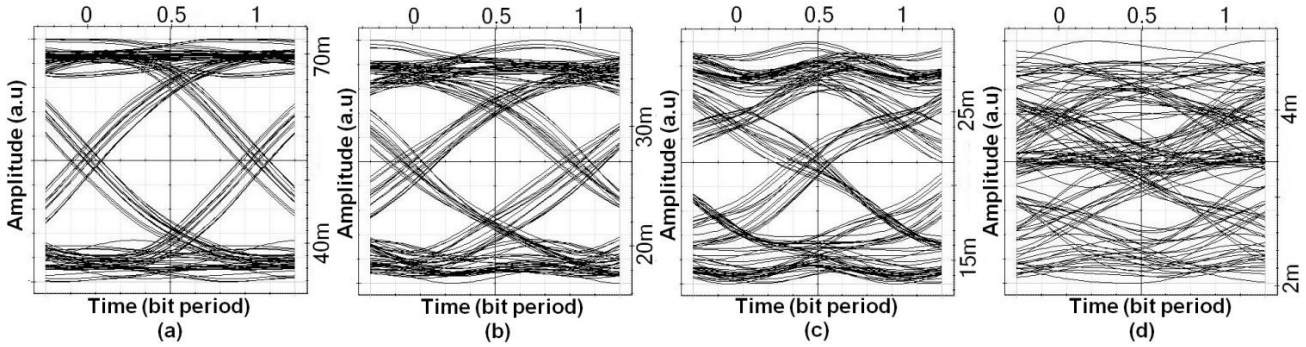

Fig.6. 4 Gbps baseband signal eye diagrams without bit walk-off effect compensation over (a) 0 km, (b) 15 km (c) 20 km (d) 60 km.

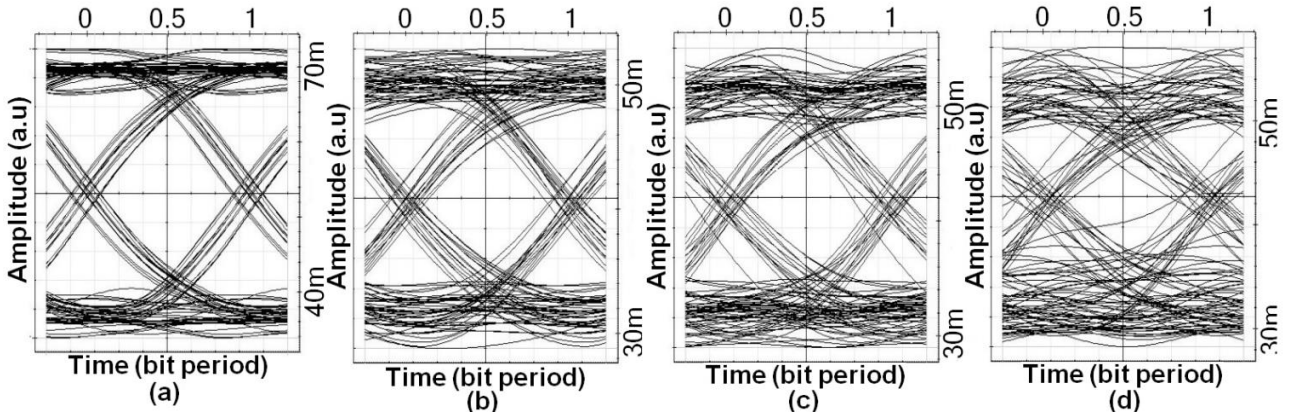

Fig.7. 4 Gbps baseband signal eye diagrams with bit walk-off effect compensation over (a) 0 km, (b) 15 km (c) 20 km (d) 60 km.

This is because only one sideband (either LSB or USB) gets modulated while the other one remains unmodulated and maintains constant amplitude and phase throughout the transmission. Hence the two tones do not

suffer from walk-off. By the use of UFBG in the system, fiber chromatic dispersion can be ameliorated which will also bring down the bit error rate. The BER curve in Fig. 8 shows that at a 0 km distance of transmission the previous system can achieve a Min. log(BER) of -9. But when the transmission distance gets increased, the BER performance gets deteriorated due to the dispersion effects and the bit walk-off effect in the fiber. While after compensating the walk-off effect in the proposed system, the BER is improved to -17.80 and the system can maintains a value of -12 after 15 km and about -6.46 at larger distances up to 60 km which proves that the BER performance is improved.

5. Conclusion

In this work, a novel method for the full-duplex generation of mm-wave signals with better transmission performance is developed. A UFBG based AOTF is employed for the tunable mm-wave signal generation of different frequency bands. The novelty of this work lies in the technique of modulating different mm-wave bands with different information and implementing a bit walk-off effect compensation in this UFBG based AOTF method of full duplex mm-wave signal generation to improve the downlink transmission performance. This scheme provides three band wireless access for the user terminal simultaneously and hence it is sufficient enough to satisfy various applications such as automotive radarsystems, WPAN links, wireless HD video streaming and also some scientific and medical unlicensed applications, with different mm-wave frequency bands carry different information at the required data rate according to the application. Moreover, the use of FBG reduces the dispersion effects in the fiber as it introduces a time delay thatwould compensate the difference in velocity of propagation of different spectral components in the pulse which causes pulse broadening. Thus high data rates up to 5 Gbps can be achieved. This method also reduces the frequency prerequisite of the oscillator and modulator greatly. The bit walk-off effect problem is addressed and compensated which improves the efficiency of the system by increasing the downlink transmission distance up to 60 km in place of 15 km offered by the system without compensation. From the simulation results, it can beshown that BER performance of the proposed system was -17.80 at 0 km fiber distance which may be degraded as distance increases but the bit walk-off effect compensation in the proposed system maintains anacceptable value of -12 at 15 km and -6.46 at 60 km distance which proves the improvement in transmission performance.

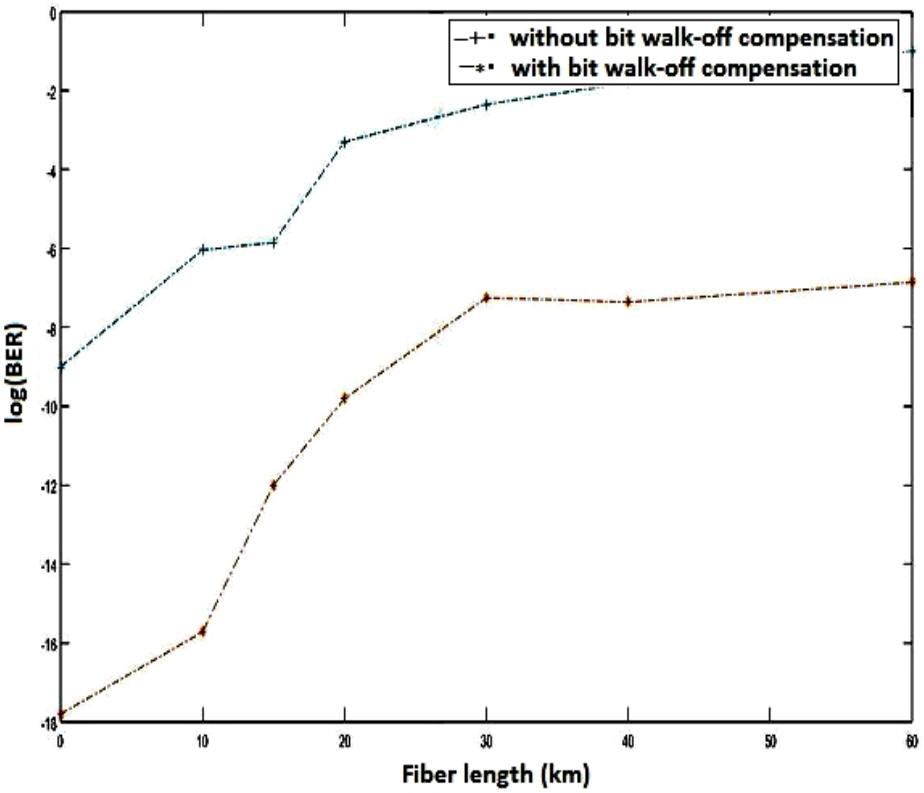

Fig. 8. Comparison of BER curves obtained with and without bit walk-off effect compensation

References

[1] M. Xiao, S. Mumtaz, Y. Huang, L. Dai, Y. Li, M. Matthaiou, IEEE Journal on Selected Areas in Communications **35**(9), 1909 (2017).

[2] A. H. M. R. Islam, M. Bakaul, A. Nirmalathas, G. E. Town, IEEE Photonics Technology Letters **23**(8), 459 (2011).

[3] N. Mohamed, S. M. Idrus, A. B. Mohammad, IEEE International RF and Microwave Conference, 326 (2008).

[4] H. Shams, P. M. Anandarajah, P. Perry, L. P. Barry, IEEE Transactions on Microwave Theory and Techniques **58**(11), 3372 (2010).

[5] M. Bhattacharya, B. Sarkar, T. Chattopadhyay, IEEE Photonics Technology Letters **14**(11), 1611 (2002).

[6] Anand Prem, Aravind Chakrapani, Advances in Natural and Applied Sciences **11**, 1998 (2017).

[7] J. Lu, Z. Dong, L. Chen, J. Yu, S. Wen, Optics Communications **281**(19), 4889 (2008).

[8] C. T. Lin, P. T. Shih, J. Chen, P. C. Peng, S. P. Dai, W. Q. Xue, S. Chi, Conference on Optical Fiber Communication/National Fiber OpticEngineers Conference, 1 (2008).

[9] Jianxin Ma, Xiangjun Xin, J. Yu, Chongxiu Yu, Kuiru Wang, Huiying Huang, Lan Rao, J. Opt. Netw. **7**(10), 837 (2008).

[10] Mandeep Singh, Sanjeev Raghuwanshi, Current Applied Physics **14**, 1837 (2014).

[11] J. Ma, J. Yu, C. Yu, X. Xin, J. Zeng, L. Chen, Journal of Lightwave Technology **25**(11), 3244 (2007).

[12] C. Y. Li, H. S. Su, C. H. Chang, H. H. Lu, P. Y. Wu, C. Y. Chen, C. L. Ying, Journal of Lightwave Technology **30**(3), 298 (2012).

[13] Yu Ji, Yan Li, Fangzheng Zhang, Jian Wu, Xiaobing Hong, Kun Xu, Wei Li, Jintong Lin, Chin. Opt. Lett. **10**(04), 042501 (2012).

[14] K. E. Muthu, A. S. Raja, 2016, International Conference on Inventive Computation Technologies (ICICT) **2**, 1 (2016).

[15] K. E. Muthu, A. S. Raja, International Conference on Wireless Communications, Signal Processing and Networking (WiSPNET), 1842 (2016).

[16] K. E. Muthu, A. S. Raja, Optoelectron. Adv. Mat. **10**(11-12), 869 (2016).

[17] W. Li, J. Yao, IEEE Transactions on Microwave Theory and Techniques **58**(11), 3259 (2010).

[18] S. Pan, J. Yao, IEEE Transactions on Microwave Theory and Techniques **58**(7), 1967 (2010).

[19] L. Gao, W. Liu, X. Chen, J. Yao, Optics Letters **38**(21), 4487 (2013).

[20] Y. Wang, L. Pei, J. Li, Y. Li, IEEE Photonics Journal **9**(1), 1 (2017).

[21] J. Ma, IEEE/OSA Journal of Optical Communications and Networking **3**(2), 127 (2011).

[22] Mehedi Hasan, Ramn Maldonado-Basilio, J. Trevor Hall, Journal of Modern Optics **62**(7), 581 (2015).

[23] Esakki K. Muthu, Sivanantha A. Raja, Journal of the European Optical Society-Rapid Publications **12**(1), 24 (2016).

[24] Min Zhou, Jianxin Ma, Congxiu Yu, Xiangjun Xin, Huiying Huang, Lan Rao, Yu Zhan, Hao Liang, IEEE 13th International Conference on Communication Technology, 538 (2011).

*Corresponding author: joseph.zacharias@rit.ac.in